

Single step preparation of $\text{CeO}_2/\text{CeAlO}_3/\gamma\text{-Al}_2\text{O}_3$ by solution combustion method: Phase evolution, thermal stability and surface modification

A.S. Prakash^b, C. Shivakumara^a, M.S. Hegde^{a,*}

^a Solid State and Structural Chemistry Unit, Indian Institute of Science, Bangalore 560012, India

^b Functional Materials Division, Central Electrochemical Research Institute, Karaikudi 630006, Tamil Nadu, India

Received 2 September 2006; received in revised form 4 January 2007; accepted 20 January 2007

Abstract

Phase evolution of $\text{CeO}_2/\gamma\text{-Al}_2\text{O}_3$ system synthesized from single step solution combustion method is examined here. The nominal compositions of ceria and alumina in $(\text{CeO}_2)_x/(\text{Al}_2\text{O}_3)_{1-x}$ are varied from $x=0.0$ to 0.66 to yield end compositions, $\gamma\text{-Al}_2\text{O}_3$ to stoichiometric CeAlO_3 phase. For the composition $x=0$, the phase formed is $\gamma\text{-Al}_2\text{O}_3$, and for $x=0.2$, CeAlO_3 is formed over $\gamma\text{-Al}_2\text{O}_3$. As the cerium content increased beyond $x=0.2$, $\text{CeO}_2/\text{CeAlO}_3/\gamma\text{-Al}_2\text{O}_3$ oxides are formed. Heating $\text{CeAlO}_3/\gamma\text{-Al}_2\text{O}_3$ in air above 700 °C resulted in transformation to $\text{CeO}_2/\gamma\text{-Al}_2\text{O}_3$ and the subsequent reduction in H_2 gave back $\text{CeAlO}_3/\gamma\text{-Al}_2\text{O}_3$. TEM studies showed CeAlO_3 crystallites growth on $\gamma\text{-Al}_2\text{O}_3$ and the oxidized sample showed CeO_2 formation over CeAlO_3 , which in turn interfaced with $\gamma\text{-Al}_2\text{O}_3$ phase. XPS analysis of $\text{CeAlO}_3/\gamma\text{-Al}_2\text{O}_3$ phase showed the presence of Ce in +3 and +4 state indicating surface oxidized CeAlO_3 phase. Epitaxial relation for growth of CeAlO_3 over $\gamma\text{-Al}_2\text{O}_3$ and CeO_2 over CeAlO_3 is demonstrated in the study, where adhesion of CeO_2 over $\gamma\text{-Al}_2\text{O}_3$ is via CeAlO_3 phase at the interface.
© 2007 Elsevier B.V. All rights reserved.

Keywords: Solution combustion synthesis; CeAlO_3 ; Cerium oxides; Solid–solid interfaces

1. Introduction

The $\text{CeO}_2\text{-Al}_2\text{O}_3$ system is of special interest in catalysis because of its technological importance in auto exhaust catalysis. Ceria is an active component of auto exhaust catalyst which is known to improve catalyst performance and also have following beneficial effects: (a) CeO_2 improves dispersion of noble metal [1–3]; (b) it improves thermal stability of $\gamma\text{-Al}_2\text{O}_3$ towards thermal sintering [2,4]; (c) enhances oxygen storage capacity (OSC) of the catalyst [2,5,6]; (d) enhances water–gas shift reaction [1,7] and (e) helps in decomposition of nitrogen oxides [8]. For ceria to serve as an oxygen storage component, it is essential that the reversible reaction between Ce^{4+} and Ce^{3+} takes place easily [2,9]. Haneda et al. [10] have reported the preparation of three kinds of cerium oxides, CeO_2 , $\text{CeO}_{2-x}/\text{Al}_2\text{O}_3$ and $\text{CeAlO}_3/\text{Al}_2\text{O}_3$ and they have showed a decrease in OSC value in the order finely-divided $\text{CeO}_{2-x} > \text{CeAlO}_3 > \text{small-sized CeO}_2 > \text{large CeO}_2$ crystallites. Shyu et al. [11] and Normand et al. [12] have reported that when ceria is dispersed

on $\gamma\text{-Al}_2\text{O}_3$ a large fraction of the cerium ions appear to be in the +3 state without any reducing atmosphere, such as H_2 . Though equilibrium solubility of CeO_2 in Al_2O_3 is limited, formation of CeAlO_3 phase is possible on the surface. Reduction of ceria on alumina in H_2 involves at least two reactions, namely, formation of non-stoichiometric cerium oxides [9,13] and cerium aluminate (CeAlO_3), depending on ceria loading [13,14].

Ways to improve the three-way catalysts performance could be devised if a better understanding could be gained on the interaction of ceria with alumina and the way it influence the properties of noble metal dispersion. Here we report the structural evolution of phases with ceria loading over $\gamma\text{-Al}_2\text{O}_3$ during the combustion synthesis and their thermal stability and surface modification on oxidizing and reducing atmospheres.

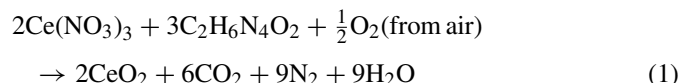
2. Experimental

2.1. Synthesis

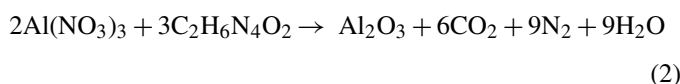
All the samples studied here are prepared by solution combustion method. The method involves exothermic redox reaction between oxidizers, generally metal nitrates and an organic fuel to yield the final product. The stoichiometry of metal nitrates to fuel

* Corresponding author. Tel.: +91 80 2293 2614; fax: +91 80 2360 1310.
E-mail address: mshegde@sscu.iisc.ernet.in (M.S. Hegde).

is calculated assuming the complete combustion to yield corresponding metal oxide and CO₂, N₂, H₂O as by-products [15,16]. For example, chemical reaction for the formation of CeO₂ and Al₂O₃ using corresponding metal nitrates and oxalyldihydrazide (ODH) can be written as follows.



Similarly,



Typical synthesis for the phases studied here are as follows.

2.1.1. $\gamma\text{-Al}_2\text{O}_3$

$\gamma\text{-Al}_2\text{O}_3$ has been prepared by the combustion of a redox mixture containing $\text{Al}(\text{NO}_3)_3 \cdot 9\text{H}_2\text{O}$ and oxalyldihydrazide $\text{C}_2\text{H}_6\text{N}_4\text{O}_2$ (ODH). In a typical preparation, 10 g of $\text{Al}(\text{NO}_3)_3 \cdot 9\text{H}_2\text{O}$ and 3.8 g (80% of stoichiometric amount) of ODH were dissolved in 15 cm³ of water in a borosilicate dish of 130 cm³ capacity. The resulting solution obtained was introduced into a muffle furnace preheated to 500 °C. The solution boiled with frothing and ignited into a flaming combustion to yield a voluminous product.

2.1.2. $(\text{CeO}_2)_x/(\gamma\text{-Al}_2\text{O}_3)_{1-x}$

The compounds $(\text{CeO}_2)_x/(\gamma\text{-Al}_2\text{O}_3)_{1-x}$ ($x=0.05, 0.10, 0.15, 0.20, 0.25, 0.30, 0.40$ and 0.66), were synthesized by the combustion of required mole ratios of $\text{Ce}(\text{NO}_3)_3 \cdot 6\text{H}_2\text{O}$, $\text{Al}(\text{NO}_3)_3 \cdot 9\text{H}_2\text{O}$ and stoichiometric amount of fuel, ODH. For the preparation of the compound with composition, say $x=0.2$, a mixture of $\text{Al}(\text{NO}_3)_3 \cdot 9\text{H}_2\text{O}$, $\text{Ce}(\text{NO}_3)_3 \cdot 6\text{H}_2\text{O}$ and ODH in the mole ratio of 1.6:0.2:2.7 was taken in a borosilicate dish of 130 cm³ capacity. The reactants were dissolved in 15 cm³ of water and introduced into a preheated muffle furnace at 500 °C. The solution boiled with frothing and ignited to burn with a flame yielding a voluminous solid product within 5 min. When $(\text{CeO}_2)_x/(\gamma\text{-Al}_2\text{O}_3)_{(1-x)}$ ($x=0.2$) was taken, CeAlO_3 phase was formed as will be shown later.

The experiments are carried out in air. The organic fuels used in solution combustion method, viz., oxalyldihydrazide (ODH), has nitrogen and carboxylic groups which forms complexes with cations and anions in solution. The complexes decompose exothermically with evolution of CO₂, N₂ and H₂O. For the stoichiometric reactions this has been confirmed by mass spectrometry, and hence Eqs. (1) and (2) are correct. Evolution of N₂ from the N-containing ligand is the main reason for higher release of heat. Instant decomposition of metal nitrates give NO₂ instead of N₂. Therefore, solution combustion method is different from NO₃ decomposition [16].

The X-ray diffraction (XRD) patterns of the phases studied here were recorded on a Siemens D5005 diffractometer using Cu K α radiation. Transmission electron microscopic (TEM) studies of powders were carried out using a JEOL JEM-200CX transmission electron microscope operated at 200 kV. X-ray

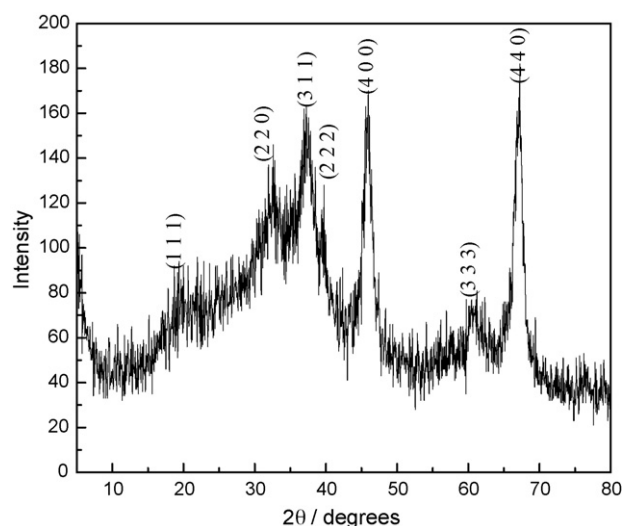


Fig. 1. Powder X-ray diffraction pattern of $\gamma\text{-Al}_2\text{O}_3$.

photoelectron spectra (XPS) of the samples were recorded on an ESCA-3 Mark II spectrometer (VG Scientific Ltd., England) using Al K α radiation (1486.6 eV). Binding energies were calculated with respect to C(1s) at 285 eV and measured with a precision of ± 0.2 eV. BET surface area of the samples was determined using Quantachrome NOVA 1000 surface area analyzer by nitrogen adsorption–desorption method at liquid nitrogen temperature.

3. Results and discussion

3.1. Structural studies

Fig. 1 shows XRD pattern of $\gamma\text{-Al}_2\text{O}_3$ synthesized by the combustion method. The pattern can be indexed to cubic phase with $a=7.912(4)$ Å. The pattern agrees well with that of $\gamma\text{-Al}_2\text{O}_3$ reported by Zhou and Snyder [17]. It should be noted here that combustion of $\text{Al}(\text{NO}_3)_3$ and urea yields $\alpha\text{-Al}_2\text{O}_3$ [18]. However, with the fuel ODH used here yielded $\gamma\text{-Al}_2\text{O}_3$ and a small amount $\alpha\text{-Al}_2\text{O}_3$ with stoichiometric $\text{Al}(\text{NO}_3)_3$ and ODH. When stoichiometric redox mixture is used maximum heat is generated. With slightly lower amount of fuel (80%), heat generated is low yielding only $\gamma\text{-Al}_2\text{O}_3$. This is how pure $\gamma\text{-Al}_2\text{O}_3$ is obtained. However, for pure $\text{CeO}_2/\text{Al}_2\text{O}_3$ composition, exact stoichiometry of nitrate and fuel is used in this study. The stabilization of meta-stable $\gamma\text{-Al}_2\text{O}_3$ during this process could be attributed to the relatively lower temperature reached during the combustion of $\text{Al}(\text{NO}_3)_3$ and ODH redox mixture.

The XRD patterns of combustion synthesized $(\text{CeO}_2)_x/(\gamma\text{-Al}_2\text{O}_3)_{1-x}$ varying x from 0.05 to 0.66 are presented in Fig. 2(a–h). For $x=0, 0.05$ and 0.1 , $\gamma\text{-Al}_2\text{O}_3$ diffraction lines are prominent. Further increase in CeO_2 mole percentage leads to the stabilization of CeAlO_3 phase. For $x=0.15$ sample, diffraction lines due to CeAlO_3 and $\gamma\text{-Al}_2\text{O}_3$ are seen. Diffraction pattern for $x=0.2$ (Fig. 2(d)) show lines mainly due to CeAlO_3 and the pattern is indexed to cubic CeAlO_3 phase. $\gamma\text{-Al}_2\text{O}_3$ is another phase that is present as can be seen from (440) diffraction line. With increasing x from 0.2 to 0.4, diffraction lines

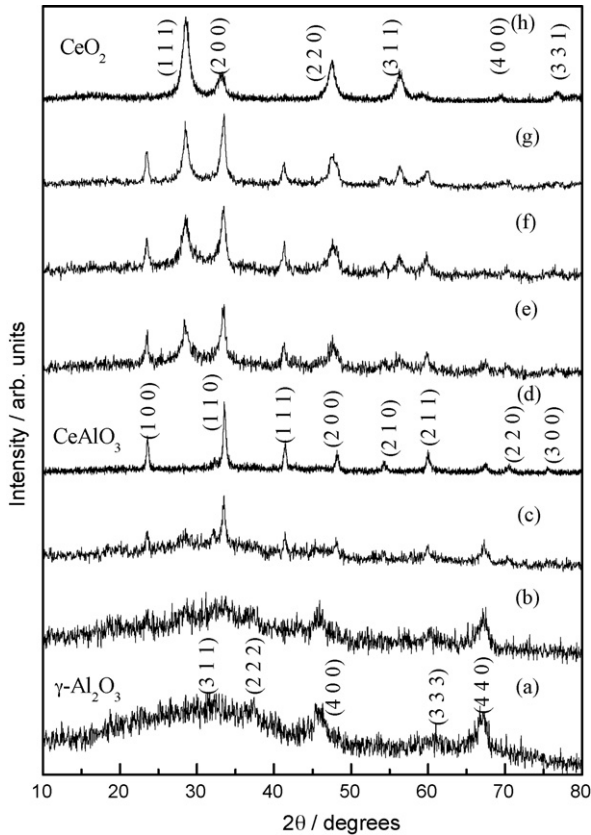


Fig. 2. X-ray diffraction patterns of $(\text{CeO}_2)_x(\text{Al}_2\text{O}_3)_{1-x}$; where x is (a) 0.05, (b) 0.10, (c) 0.15, (d) 0.20, (e) 0.25, (f) 0.30, (g) 0.40 and (h) 0.66.

corresponding to CeO_2 appear along with those of CeAlO_3 . For $x=0.66$ (Fig. 2(h)), CeO_2 lines are prominent.

CeAlO_3 has been reported to crystallize in different structures depending on the synthetic conditions followed. Mizuno et al. [19] have reported the CeAlO_3 phase close to ideal cubic perovskite structure with lattice parameter $a = 3.760 \text{ \AA}$. Shishido et al. [20] have reported the CeAlO_3 structure of tetragonal symmetry with $a = 3.7669(9) \text{ \AA}$ and $c = 3.7967(7) \text{ \AA}$, while Kim [21] reported it to be crystallizing in rhombohedral symmetry with $a = 5.327 \text{ \AA}$ and $\alpha = 60.15^\circ$. In a recent study, Fu and Ijdo [22] showed structural phase transition of CeAlO_3 . The crystal structure changes from tetragonal to orthorhombic to rhombohedral to cubic phases when heated from 300 to 1423 K. The distortion from cubic to rhombohedral symmetry as well as to tetragonal symmetry is very small. The diffraction lines of the compounds reported here are broad and the lines can be indexed to a pseudo cubic perovskite with $a \sim 3.772(5) \text{ \AA}$. Thus, at $x=0.2$, pseudo cubic CeAlO_3 phase is formed and the excess alumina present is in the $\gamma\text{-Al}_2\text{O}_3$ phase. Flame temperature in the combustion synthesis is $\sim 1000^\circ\text{C}$. The product formed is quenched to 500°C in a few seconds. Therefore, formation of pseudo cubic CeAlO_3 phase is expected.

3.2. Thermal stability of $\text{CeAlO}_3/\gamma\text{-Al}_2\text{O}_3$

To study the stability of CeAlO_3 in $\gamma\text{-Al}_2\text{O}_3$ matrix the sample containing CeAlO_3 ($x=0.2$) was calcined in air at dif-

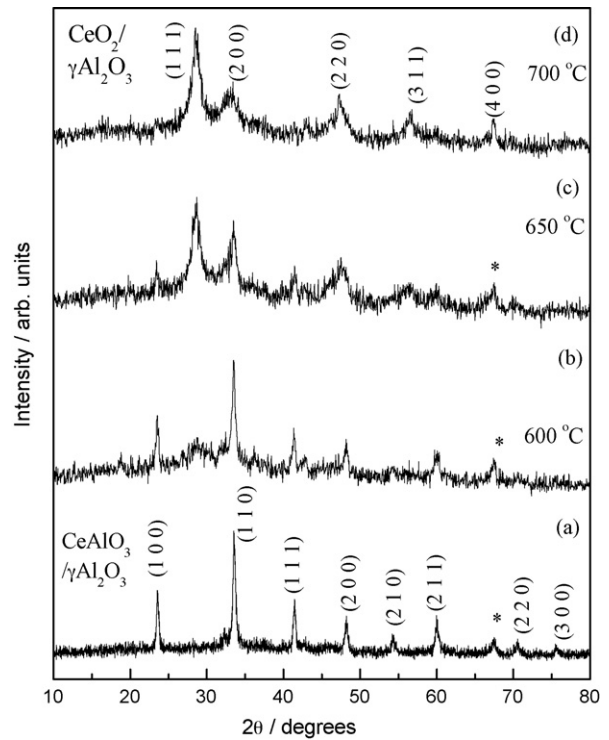


Fig. 3. Powder XRD pattern of the products formed from decomposition of $\text{CeAlO}_3/\gamma\text{-Al}_2\text{O}_3$ with temperature: (a) 500°C , (b) 600°C , (c) 650°C and (d) 700°C . Asterisk (*) denotes 100% diffraction line of $\gamma\text{-Al}_2\text{O}_3$.

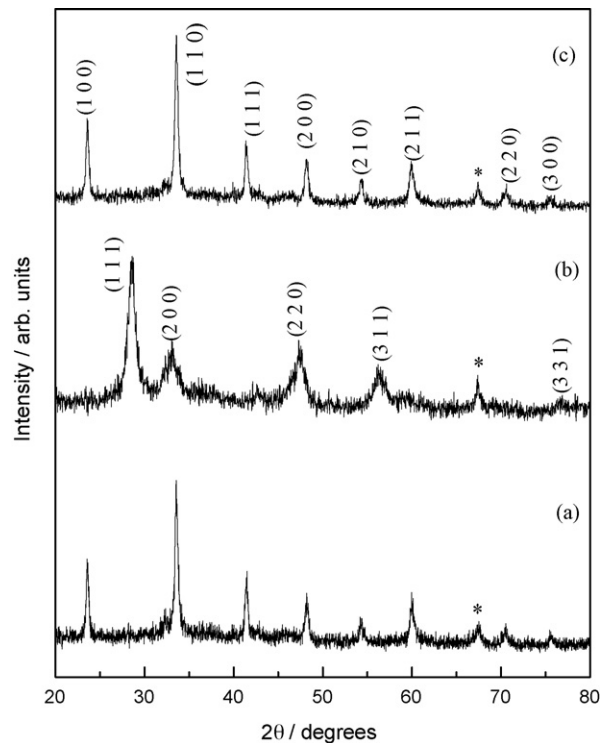


Fig. 4. Powder X-ray diffraction patterns of $\text{CeAlO}_3/\gamma\text{-Al}_2\text{O}_3$ under different conditions: (a) as-synthesized, (b) heated in air at 700°C for 8 h and (c) after reduction in H_2 at 750°C for 8 h. Asterisk (*) denotes 100% diffraction line of $\gamma\text{-Al}_2\text{O}_3$.

ferent temperatures from 300 to 800 °C. At each temperature the dwelling time was 8 h. The XRD pattern of the products formed are shown in Fig. 3(a–d). CeAlO₃ phase formed (for $x=0.2$ sample) was stable up to 500 °C and on heating to higher temperature, CeO₂ phase started appearing. Sintering at 600 °C resulted in the oxidation and decomposition of CeAlO₃ giving CeO₂ and γ -Al₂O₃. Broad diffraction lines corresponding to CeO₂ along with diffraction lines of CeAlO₃ and γ -Al₂O₃ are seen in Fig. 3(b). The Intensities of the diffraction lines due to CeO₂ increased with increase in calcination temperature. Calcination at 700 °C resulted in the decomposition of CeAlO₃ to CeO₂ and γ -Al₂O₃. Since intensity of lines due to γ -Al₂O₃ are low compared to CeO₂ due to large difference in the atomic scattering factors of Al and Ce, only the γ -Al₂O₃ (440) line is identified. The diffraction lines corresponding to CeO₂ are broad and the average crystallite sizes calculated from Scherrer method are in the range of 5–7 nm. The product obtained after calcinations at 700 °C in air was reduced in H₂ at 750 °C for 8 h. CeAlO₃ phase (not shown here) is formed indicating the conversion of CeAlO₃ to CeO₂ is reversible.

Fig. 4 shows XRD patterns of (a) as-synthesized, (b) oxidized and (c) reduced CeAlO₃/ γ -Al₂O₃. As-synthesized material shows the CeAlO₃ phase formation. Calcination at 700 °C resulted in the oxidation of CeAlO₃ to CeO₂. Reduction of CeO₂/ γ -Al₂O₃ in H₂ at 750 °C restores the CeAlO₃ phase completely.

3.3. TEM studies

To confirm the X-ray data and to study the morphology of the particles, TEM study was undertaken. Fig. 5(a and b) shows TEM bright field images and corresponding electron diffraction patterns of as synthesized CeAlO₃/ γ -Al₂O₃. The dark regions in the micrograph, shown in Fig. 5(a) correspond to the CeAlO₃ crystallites. Electron diffraction pattern obtained from the CeAlO₃ crystallites (Fig. 5(b)) clearly demonstrates cubic CeAlO₃ phase along with ring patterns of γ -Al₂O₃. CeO₂ phase is not identified either in the ring pattern or in the diffraction spots. Distinct square diffraction patterns observed here are due to the CeAlO₃ phase.

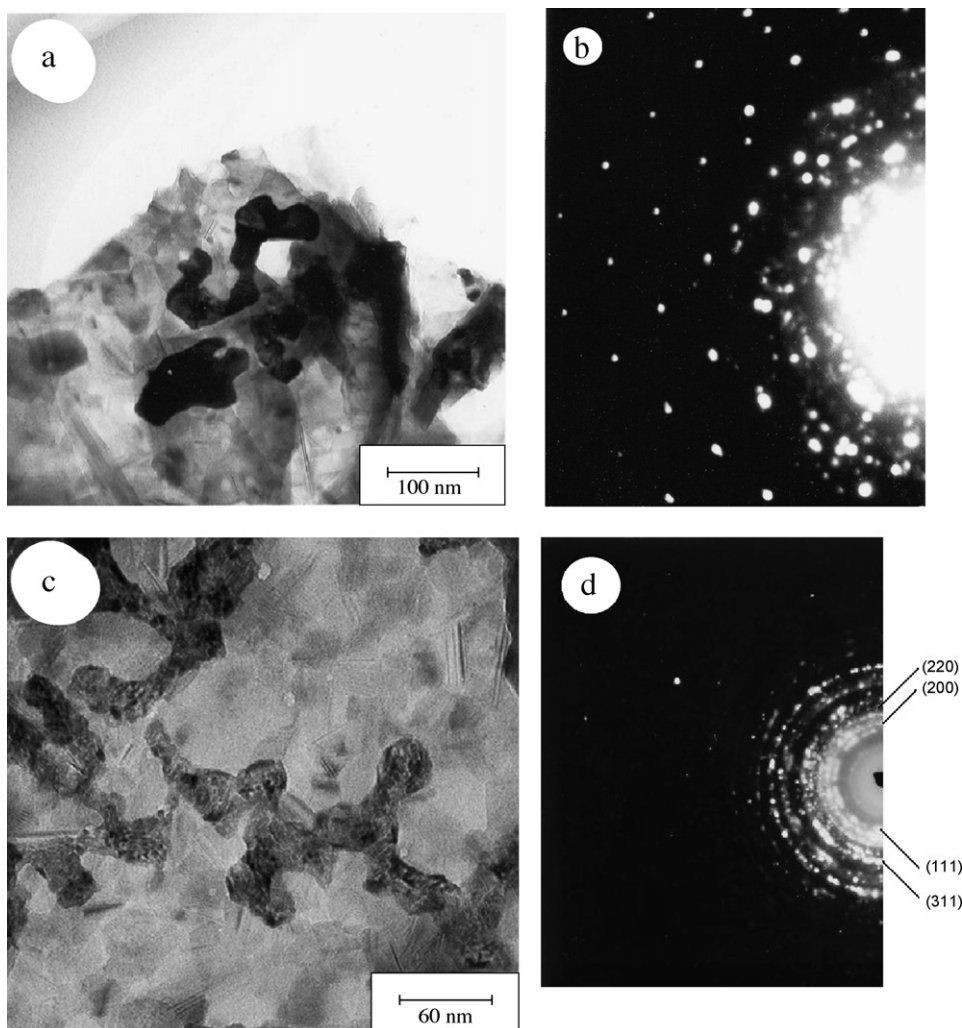


Fig. 5. TEM images of (a) as-synthesized CeAlO₃/ γ -Al₂O₃, (b) ED pattern of CeAlO₃, (c) CeAlO₃/ γ -Al₂O₃ (oxidized at 700 °C) and (d) ED pattern of oxidized CeAlO₃/ γ -Al₂O₃.

Fig. 5(c and d) shows TEM micrographs and electron diffraction pattern of $\text{CeO}_2/\gamma\text{-Al}_2\text{O}_3$ which was obtained by heating $\text{CeAlO}_3/\gamma\text{-Al}_2\text{O}_3$ at 700°C in air. The micrographs show small clusters of CeO_2 particles segregated on $\gamma\text{-Al}_2\text{O}_3$ surface as bi-dimensional ceria patches. Morphology confirms the growth of CeO_2 over CeAlO_3 . The TEM images show small and thin cerium oxide particles, indicating that the small CeO_2 crystallites are formed out of CeAlO_3 phase. Diffraction pattern shows ring patterns corresponding to the d spacing of CeO_2 ($\sim 1.91, 1.63, 1.57$ and 1.35 \AA) along with less intense diffused rings corresponding to $\gamma\text{-Al}_2\text{O}_3$ phase. Either rings or clean diffraction spots due to CeAlO_3 is not seen in the oxidized material.

3.4. XPS studies

A detailed XPS study of these oxide phases were carried out. We show in Fig. 6, Ce(3d) region of pure CeO_2 (curve (a)), as-prepared $\text{CeAlO}_3/\gamma\text{-Al}_2\text{O}_3$ (curve (b)) and $\text{CeAlO}_3/\gamma\text{-Al}_2\text{O}_3$ oxidized ex situ in air, curve (c). The same sample was reduced in H_2 and Ce(3d) region of the reduced sample is shown in Fig. 6(d). Ce^{4+} (3d) spectrum in CeO_2 is characteristic of strong satellites at 889.1, 898.8 and 908.2, 917.2 eV. All the $\text{CeAlO}_3/\gamma\text{-Al}_2\text{O}_3$ phases, whether in oxidized or reduced form shows distinct spectral features compared to CeO_2 . Both the shape and intensity of satellites of Ce(3d) spectrum in these samples are indicative of Ce in +3 and +4 state. Therefore, a detailed analysis of Ce(3d) region was carried out for as-prepared $\text{CeAlO}_3/\gamma\text{-Al}_2\text{O}_3$ and for pure CeO_2 . In Fig. 7(a), we show Ce(3d) deconvoluted spectrum of Ce in CeO_2 . The satellites and the main peaks are clearly iden-

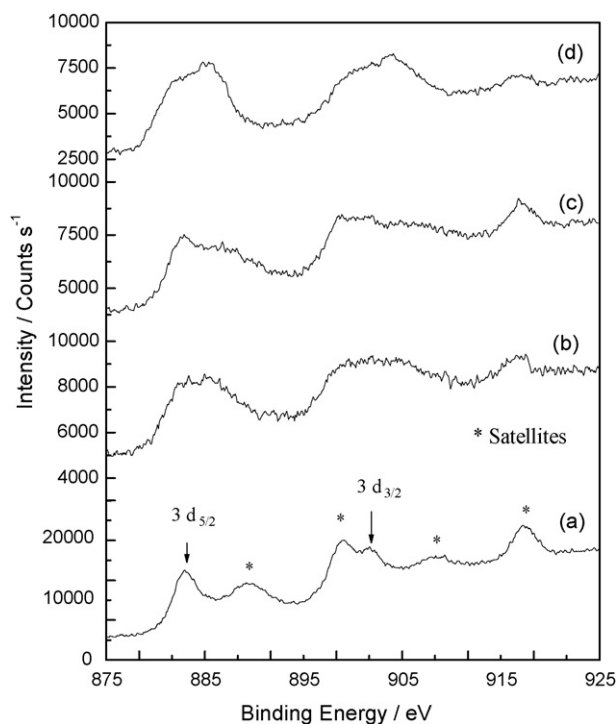


Fig. 6. X-ray photoelectron spectra of Ce(3d) core level region in (a) as synthesized CeO_2 , (b) as synthesized $\text{CeAlO}_3/\gamma\text{-Al}_2\text{O}_3$, (c) oxidized $\text{CeAlO}_3/\gamma\text{-Al}_2\text{O}_3$ and (d) reduced $\text{CeAlO}_3/\gamma\text{-Al}_2\text{O}_3$. Asterisk (*) indicates the satellites due to Ce^{4+} ion.

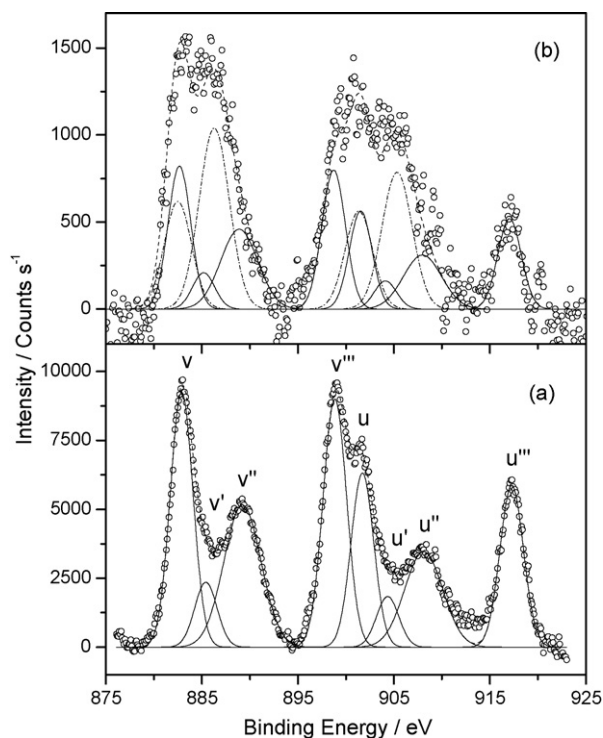


Fig. 7. Deconvoluted XP spectrum of Ce(3d) in (a) CeO_2 (deconvoluted peaks (vv', v'', v''') for $\text{Ce}(3d_{5/2})$ and (uu', u'', u''') for $\text{Ce}(3d_{3/2})$) and (b) $\text{CeAlO}_3/\gamma\text{-Al}_2\text{O}_3$. Full line for CeO_2 and dash-dot for CeAlO_3 .

tified in the CeO_2 spectra and it agrees with those reported in the literature [23,24]. Ce(3d) region of as-prepared $\text{CeAlO}_3/\gamma\text{-Al}_2\text{O}_3$ has been fitted to both Ce^{3+} and Ce^{4+} and XPS in Fig. 7(b) corresponds to Ce_2O_3 and CeO_2 [11]. In the analysis, the total intensity of the Ce^{4+} satellite at $\sim 917 \text{ eV}$ was taken as the reference and the rest of the peaks due to Ce^{4+} were generated which corresponded to pure CeO_2 spectra as shown in Fig. 7(a). As can be seen from the Fig. 7(b), the difference can be taken care of by fitting the difference spectra to Ce^{3+} (3d) state [25]. Relative intensities of the main peak and the satellites due to Ce^{3+} in the spectra agree well with the XPS of Ce_2O_3 [25]. Thus, the Ce(3d) region of $\text{CeAlO}_3/\gamma\text{-Al}_2\text{O}_3$ contains both Ce^{3+} and Ce^{4+} features. The relative intensity value of Ce^{3+} to Ce^{4+} obtained from the integrated area is ~ 0.46 . Ce^{3+} states in the XPS of as synthesized catalysts are then due to Ce^{3+} in CeAlO_3 since Ce_2O_3 phase is not detected in the XRD. Therefore, the surface of the $\text{CeAlO}_3/\gamma\text{-Al}_2\text{O}_3$ contains CeO_2 , this is not detected in XRD studies. A similar analysis of H_2 reduced sample gave much less intensity due to Ce^{4+} as can be seen from Fig. 6(d). Thus, XPS analysis of the as-synthesized $\text{CeAlO}_3/\gamma\text{-Al}_2\text{O}_3$ contains Ce in +3 state corresponding to CeAlO_3 phase and Ce^{4+} state corresponding to CeO_2 on the surface.

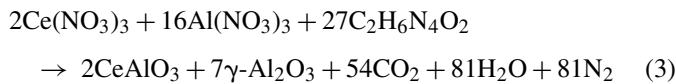
Binding energy of Al(2p) is observed at 74.1 eV, which corresponds to Al in +3 state as in Al_2O_3 . O(1s) region was also looked into and the peak was broad centered at $\sim 531 \text{ eV}$. The O(1s) region in pure CeO_2 is narrow and the peak position is at $\sim 530.5 \text{ eV}$. The shift of the binding energy by $\sim 0.5 \text{ eV}$ can be attributed to contribution from alumina in the $\text{CeAlO}_3/\gamma\text{-Al}_2\text{O}_3$ system.

3.5. Surface area analysis

BET surface area of as-synthesized and heat-treated samples has been measured to understand the segregation of the phase as CeO_2 or CeAlO_3 . The surface areas varied from 50 to $60 \text{ m}^2/\text{g}$, regardless of whether the phase is CeO_2 or CeAlO_3 and there was no significant change in surface area was observed after repeated reduction and oxidation cycles at 700°C .

3.6. Formation of $\text{CeO}_2/\text{CeAlO}_3/\gamma\text{-Al}_2\text{O}_3$

When stoichiometric amount of Ce either in +3 or in +4 state (as precursors) and $\text{Al}(\text{NO}_3)_3$ in 1:1 ratio reacted with required amount fuel, the products formed are CeO_2 and $\gamma\text{-Al}_2\text{O}_3$ and not CeAlO_3 . However, when a nitrate mixture containing Ce:Al in the atomic ratio of 2:16, CeAlO_3 and $\gamma\text{-Al}_2\text{O}_3$ phases are formed. The reaction can be written as follows:



With increase of x taken for the preparation of $\text{In}(\text{CeO}_2)_x/(\gamma\text{-Al}_2\text{O}_3)_{1-x}$ CeAlO_3 phase is formed. Maximum amount of CeAlO_3 is found for the Ce:Al ratio of 2:16.

XRD and TEM study indeed confirm the formation of CeAlO_3 phase along with $\gamma\text{-Al}_2\text{O}_3$. XPS study of the as-prepared sample containing maximum amount of CeAlO_3 showed Ce in +3 as well as +4 state. From all the experimental proofs gathered in this study, we attribute Ce^{4+} presence to the surface oxidation of CeAlO_3 to CeO_2 phase. This is confirmed by the presence of mostly Ce^{3+} state in the hydrogen reduced sample.

3.7. $\text{CeO}_2/\text{CeAlO}_3/\gamma\text{-Al}_2\text{O}_3$ solid–solid interfaces

$\gamma\text{-Al}_2\text{O}_3$ crystallizes in defect spinel structure with cubic a parameter of $7.911(2) \text{ \AA}$. Rietveld analysis has indicated site occupancy of Al ions in $\gamma\text{-Al}_2\text{O}_3$ crystallizing in $Fd\bar{3}m$ space group [17]. Accordingly, instead of 32 oxide ions and 24 cations in the normal spinel unit cell, $\gamma\text{-Al}_2\text{O}_3$ showed 32 oxide ions, 16 Al ions in the octahedral positions and about 5.5 Al ions in the tetrahedral sites indicating Al ion vacancy in the tetrahedral sites [17]. The $a/2$ of $\gamma\text{-Al}_2\text{O}_3$ (3.95 \AA) is close to the lattice parameter a (3.772 \AA) of CeAlO_3 . Therefore, it is possible to consider the growth of CeAlO_3 over $\gamma\text{-Al}_2\text{O}_3$. This is shown in Fig. 8(a). Lattice mismatch between $a/2$ of $\gamma\text{-Al}_2\text{O}_3$ ($1/2a$) and a of CeAlO_3 is less than 5%. Indeed, epitaxial growth of $\text{YBa}_2\text{Cu}_3\text{O}_7$ ($a = 3.83 \text{ \AA}$, $b = 3.89 \text{ \AA}$ and $c = 11.65 \text{ \AA}$) in the c -direction is achieved on sapphire with $1\bar{1}02$ with cubic a parameter of 3.64 \AA [26]. Lattice mismatch between CeAlO_3 and $\gamma\text{-Al}_2\text{O}_3$ is even smaller than between sapphire ($1\bar{1}02$) surface and a or b of $\text{YBa}_2\text{Cu}_3\text{O}_7$. Therefore, growth of cubic CeAlO_3 over cubic $\gamma\text{-Al}_2\text{O}_3$ as shown in Fig. 8(a) is feasible.

CeAlO_3 crystallizes in pseudo cubic perovskite structure with lattice parameter $a = 3.772(5) \text{ \AA}$. This structure can be viewed as layers containing $(\text{CeO})\text{--}(\text{AlO}_2)\text{--}(\text{CeO})\text{--}(\text{AlO}_2)$. Lattice

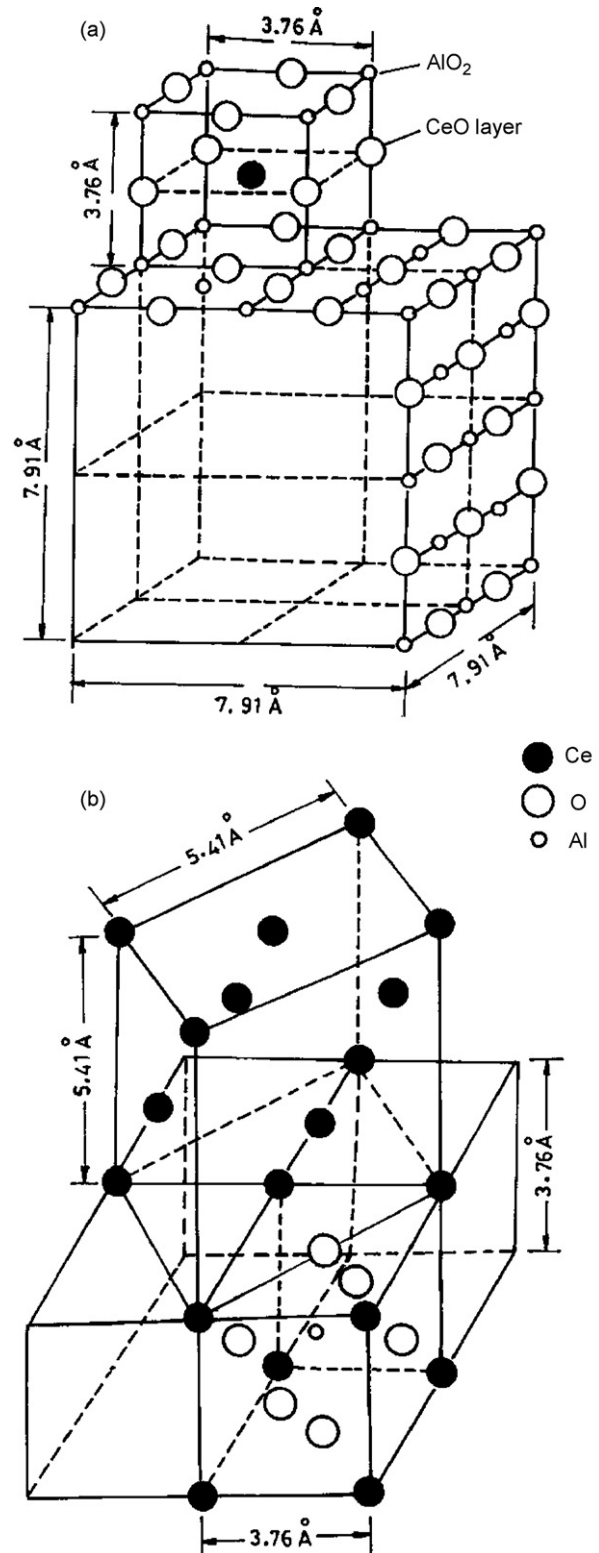


Fig. 8. Schematic representation of epitaxial growth of (a) CeAlO_3 over $\gamma\text{-Al}_2\text{O}_3$ and (b) CeAlO_3 over CeO_2 .

parameter of CeO_2 , $a = 5.41 \text{ \AA}$ and $\sqrt{2}a_0(\text{CeAlO}_3) \approx a(\text{CeO}_2)$. Conversely, $a/\sqrt{2}$ of CeO_2 is close to the lattice parameter of CeAlO_3 . Therefore, it is possible to construct CeAlO_3 over CeO_2 or CeO_2 over CeAlO_3 as given in Fig. 8(b).

On heating, CeAlO₃ decomposes into γ -Al₂O₃ and CeO₂. On reduction γ -Al₂O₃ and CeO₂ react in this nano volume giving back CeAlO₃.

The reaction can be written as follows:



Therefore, formation of CeAlO₃ phase on γ -Al₂O₃, formation of CeO₂ and γ -Al₂O₃ on heating and CeAlO₃ formation upon reduction in H₂ atmosphere are facilitated by the structural relation between CeO₂–CeAlO₃– γ -Al₂O₃. It is striking to find CeAlO₃ growth over γ -Al₂O₃ for $x=0.2$ composition. Almost all the Ce taken is converted to CeAlO₃ phase. For CeAlO₃ growth Ce:Al atomic ratio required is 2:16. Purely by experimental studies, 30 wt.% CeO₂ in γ -Al₂O₃ is arrived for a best CeO₂/ γ -Al₂O₃ catalyst followed by noble metal impregnation [27]. 30 wt.% CeO₂ in γ -Al₂O₃ corresponds to 20 mol% CeO₂ and 80 mol% γ -Al₂O₃ that is, (Al₂O₃)_{0.80}(CeO₂)_{0.20}. This composition indeed gave CeAlO₃/ γ -Al₂O₃ phase in our studies (Eq. (3)). We believe that CeAlO₃ growth on γ -Al₂O₃ is a constrained growth due to lattice matching and such a good growth takes place for 2:16 composition.

4. Conclusions

The multicomponent system CeO₂/CeAlO₃/ γ -Al₂O₃ is a presently employed catalyst support for three-way auto exhaust catalysis which is synthesized by a single step solution combustion synthesis. For the composition Ce:Al in 2:16, which corresponds to 20 mol% CeO₂ in γ -Al₂O₃, the phase observed is CeAlO₃ over γ -Al₂O₃. More than 20 mol% CeO₂ composition resulted in segregation of CeO₂ phase. CeAlO₃ transforms to CeO₂ and γ -Al₂O₃ on heating in air above 700 °C which converts back to CeAlO₃ on H₂ reduction. Reversible formation of CeAlO₃ \leftrightarrow CeO₂ + γ -Al₂O₃ on oxidation–reduction retains the effective surface area. XPS studies showed the presence of Ce⁴⁺ in CeAlO₃/ γ -Al₂O₃, formed due to the surface oxidation of CeAlO₃. The CeO₂ crystallites formed over γ -Al₂O₃ are of the size 20–30 nm, whereas CeAlO₃ crystallites dispersed in γ -Al₂O₃ are of 80–100 nm. Adhesion of CeO₂ to γ -Al₂O₃ is due to epitaxial growth of CeAlO₃ over γ -Al₂O₃ and CeO₂ over CeAlO₃.

Acknowledgements

Financial support from the Department of Science and Technology (DST), Government of India, is gratefully acknowledged. Authors thank Late Dr. G.N. Subanna, for microscopic investigations of the samples.

References

- [1] J.C. Summers, S.A. Ausen, J. Catal. 58 (1979) 131.
- [2] H.C. Yao, Y.F. Yu-Yao, J. Catal. 86 (1984) 254.
- [3] E.C. Su, C.N. Montreuil, W.G. Rothchild, Appl. Catal. 17 (1985) 75.
- [4] M. Ozawa, M. Kimura, J. Mater. Sci. Lett. 9 (1990) 291.
- [5] N. Kakuta, N. Morishima, M. Kotobuki, T. Iwase, T. Mizushima, Y. Sato, S. Matsuura, Appl. Surf. Sci. 121/122 (1997) 408.
- [6] B. Engler, E. Koberstein, P. Schubert, Appl. Catal. 48 (1989) 71.
- [7] T. Shido, Y. Iwasawa, J. Catal. 136 (1992) 493.
- [8] A. Martinez-Arias, J. Soria, J.C. Conesa, X.L. Seoane, A. Arcoya, R. Cataluna, J. Chem. Soc. Faraday Trans. 91 (1995) 1679.
- [9] N. Kaufherr, L. Mendelovici, J. Less-Common Met. 107 (1985) 281.
- [10] M. Haneda, T. Mizushima, N. Kakuta, A. Ueno, Y. Sato, S. Matsuura, K. Kasahara, M. Sato, Bull. Chem. Soc. Jpn. 66 (1993) 1279.
- [11] J.Z. Shyu, W.H. Webber, H.S. Gandhi, J. Phys. Chem. 92 (1988) 4964.
- [12] F.L. Normand, L. Hilaire, K. Kili, G. Krill, G. Maire, J. Phys. Chem. 92 (1988) 2561.
- [13] S. Geller, P.M. Raccach, Phys. Rev. B. 2 (1970) 1167.
- [14] P.J. Schmitz, R.K. Usman, C.R. Peters, G.W. Graham, R.W. McCabe, Appl. Surf. Sci. 72 (1993) 181.
- [15] K.C. Patil, Bull. Mater. Sci. 16 (1993) 533.
- [16] K.C. Patil, S.T. Aruna, S. Ekambaram, Curr. Opin. Solid State Mater. Sci. 2 (1997) 158.
- [17] R.S. Zhou, R.L. Snyder, Acta Cryst. B. 47 (1991) 617.
- [18] P. Bera, K.C. Patil, M.S. Hegde, Phys. Chem. Chem. Phys. 2 (2000) 373.
- [19] M. Mizuno, R. Berjoan, J.P. Coutures, M. Ferox, Y.K. Shi, J. Ceram. Assoc. Jpn. 83 (1975) 50.
- [20] T. Shishido, M. Tanaka, H. Horiuchi, H. Iwasaki, N. Toyota, D. Shindo, T. Fukuda, J. Alloys Compd. 192 (1993) 84.
- [21] Y.S. Kim, Acta Cryst. B. 24 (1968) 295.
- [22] W.T. Fu, D.J.W. Ijdo, J. Solid State Chem. 179 (2006) 2732.
- [23] P. Burroughs, A. Hammett, A.F. Orchard, G. Thorntom, J. Chem. Soc. Dalton Trans. 17 (1976) 1686.
- [24] A. Fujimori, Phys. Rev. B 27 (1983) 3992.
- [25] A. Fujimori, J. Magn. Magn. Mater. 47–48 (1985) 243.
- [26] D. Kumar, K.M. Satyalakshmi, S.S. Monohar, M.S. Hegde, Bull. Mater. Sci. 117 (1994) 625.
- [27] E.S. Lox, B.H. Engles, E. Koberstein, Technical Paper Series 910841, Society of Automotive Engineers, Warrendale, 1991.